ORIGINAL PAPER

Water Transport in Polylactide and Polylactide/Montmorillonite Composites

**An Du · Genaro A. Gelves · Donghun Koo ·
Uttandaraman Sundararaj · Richard Cairncross**

Abstract Polylactide–montmorillonite composites were
fabricated by melt-blending followed by compression
molding, and water permeability of the composites was
studied by both experiments and theoretical models. The
water permeation in composites decreases with increasing
concentration of montmorillonite. Specifically, at a con-
centration of 10 wt% of montmorillonite, the water per-
meation is 34 % less than in the neat polymer.
Transmission electron microscopy (TEM) and wide-angle
X-ray scattering (WAXS) results show that most of the
montmorillonite particles are well-dispersed and randomly
exfoliated in the polymer matrix. A fit of theoretical
models to the permeation data estimates that montmoril-
lonite platelets are mostly exfoliated in the polymer matrix
and oriented randomly, which matches with results from
WAXS and TEM.

Keywords Exfoliation · Montmorillonite · Permeation ·
Polylactide

Introduction

Bio-based polymers such as polylactide (PLA) are now
being produced commercially by several companies. Bio-
based polymers are promoted as having numerous
environmental advantages in comparison to petroleum-
based polymers [1–4]. However, there are also some
aspects of PLA that limit its displacement of petroleum-
based polymers such as polyethylene terephthalate (PET)
in packaging applications. PLA is currently having diffi-
culties in achieving good physical and mechanical prop-
erties compared to conventional synthetic polymers [5, 6].
More importantly, moisture barrier properties in PLA are
still poorly understood. In order for PLA to be competitive
to petroleum-based polymers in packaging applications, the
moisture barrier properties of PLA have to be improved.
Some researchers have attempted to improve moisture
barrier properties in PLA by chemical or physical modifi-
cations such as varying molecular weight, stereoisomerism,
end group composition, blending, coating, copolymeriza-
tion, adding microparticles or nanoparticles, chemical
surface reaction and plasma treatment [7–10]. Recently,
Koo et al. [11] showed that the water sorption in end-
capped PLA with palmityl and acetyl end groups at a
molecular weight of 10,000 and optimal heat treatment
condition was about 55 % less than water sorption in
commercially available PLA [11].

A promising method to improve moisture barrier prop-
erties is fabricating PLA composites with impermeable,
well-dispersed nanoparticles. However, the quality of dis-
persion of nanoparticles depends on the extent of com-
patibility between the nanoparticles and the polymer matrix
and can result in either a microphase-separated (interca-
lated) or an exfoliated morphology [10]. Pluta et al. [12]
prepared PLA/clay nanocomposites with 3 wt% organo-
modified montmorillonite by melt-blending technique.
Their results showed that good affinity and compatibility
between organomodified clays and the PLA matrix was
established in nanocomposites but not in microcomposites.
Gorrasi et al. [9] studied water barrier properties in both

A. Du · D. Koo · R. Cairncross (✉)
Department of Chemical and Biological Engineering, Drexel
University, 3141 Chestnut Street, Philadelphia, PA 19104-2875,
USA
e-mail: cairncross@drexel.edu

G. A. Gelves · U. Sundararaj
Department of Chemical and Petroleum Engineering,
University of Calgary, Calgary, AB T2N 1N4, Canada

intercalated and exfoliated PLA layered aluminosilicate nanocomposites. In intercalated samples, the amount of water sorption increased with the amount of aluminosilicate. However, the lowest water sorption was found in exfoliated nanocomposites. Therefore, they suggested that the exfoliation of the inorganic fillers in the continuous polymer phase plays a significant role in improving the moisture barrier properties in PLA [9]. The best improvement in permeability in PLA-based composites was reported by Zenkiewicz and Richert [13] as a 60 % reduction for a sample containing 75 wt% PLA, 5 wt% montmorillonite and 20 wt% poly(methyl methacrylate). The literature supports that there is clearly a trend of improving moisture barrier properties in PLA by making PLA-montmorillonite nanocomposites if modified clay particles are well-dispersed into the polymer matrix.

This paper documents how permeability of melt-blended poly(L-lactide) (PLLA) and PLLA–montmorillonite (PLLA–MMT) nanocomposites depends on MMT content, heat treatment, thermal properties and microstructure. Neat PLLA and PLLA–MMT composite samples were characterized by differential scanning calorimetry (DSC), thermal gravimetric analysis (TGA), wide-angle X-ray scattering (WAXS) and transmission electron microscopy (TEM) techniques. Water permeation experiments were also conducted on neat polymer and composite films at a constant temperature and relative humidity. Permeation experimental results were fit to models that correlate permeability to the shape and orientation of MMT particles. Compression-molded PLLA–MMT composite samples were also annealed at different heat treatment conditions in order to study the effect of heat treatment on water transport properties.

Theoretical Background

Several researchers have developed models to describe gas barrier properties in composite materials [14–21]. Gas barrier properties in composite materials depend on several factors, such as the concentration, shape and orientation of the fillers. The most classical model is the Maxwell model relating the effective permeability of a composite membrane to the permeabilities of the continuous phase and a dispersed phase of isolated spherical particles. However, the Maxwell model is limited to a dilute suspension of spheres and does not take into account other shapes or orientation of the fillers [17]. A few different models describing gas barrier properties in composite materials have been also developed by taking into account the shape and orientation of the fillers. The shape and orientation of fillers are key factors to improve the moisture barrier properties in polymer nanocomposites.

In general, the permeability in a composite system depends on several factors, such as: (1) the differences in the diffusivity and solubility of the dispersed and continuous phases, (2) the volume fraction of the dispersed phase, (3) the shape and arrangement of the dispersed phase which is directly related to its tortuosity, and (4) the effects of the inter-phase region between the continuous and the dispersed phase [16, 19]. In this paper, the effect of the inter-phase region is assumed to be negligible. The tortuosity factor (τ) is the ratio of the actual distance travelled by a penetrant to the shortest distance possible without the presence of the fillers. A common model that estimates permeability of a mixed matrix membrane (composite membrane) which is an extension to the Maxwell model is the Maxwell–Wagner–Sillars (MWS) model [15, 17]. The MWS model applies to a dilute dispersion of ellipsoids that are oriented along the axis of the flux direction. In the PLLA–MMT matrix, MMT is impermeable although MMT may absorb water on the surface. By assuming that the water permeability in MMT is approximately zero, the MWS model can be written as:

$$\frac{P_{eff}}{P_c} = 1 - \frac{\phi_d}{1 - n(1 - \phi_d)} = \frac{1 - \phi_d}{\tau} \tag{1}$$

where

$$\tau = \frac{1 - n(1 - \phi_d)}{1 - n} \tag{2}$$

In Eq. (1), P_c, P_{eff} and ϕ_d indicate the permeability of the continuous phase, permeability of the overall composite membrane and the volume fraction of the filler or the dispersed phase, respectively. n is the shape factor whose value is between 0 and 1. For prolate ellipsoid, n is between 0 and 1/3. For oblate ellipsoids, n is between 1/3 and 1 while $n = 1/3$ becomes the special case of Maxwell model prediction for spherical filler particles [15–19].

An alternate model of permeability in composites containing sheet-like fillers was derived by Bharadwaj [14]. In Bharadwaj's model, the composite particles have dimensions of $L \times W$ where L and W represent the length and width of the particles. Bharadwaj's model can be rearranged to determine the shape factor, n, in the MWS model with the assumption that the water permeability in MMT particles is approximately zero.

$$n = \frac{\frac{L}{3W}\left(S + \frac{1}{2}\right)}{1 + \frac{L}{3W}\left(S + \frac{1}{2}\right)} \tag{3}$$

and

$$\tau = 1 + \frac{L}{2W} \phi_d \frac{2}{3} \left(S + \frac{1}{2}\right) \tag{4}$$

L/W is the aspect ratio of the fillers and S is an order parameter defined as:

$$S = \frac{1}{2}\left(3\cos^2\theta - 1\right) \tag{5}$$

In Eq. (5), θ is the angle between the direction of permeation and the normal to the surface of the filler particles [14]. S can have any value between $-1/2$ and 1 depending on the orientation of the filler. The ideal case for the best moisture barrier properties of the composites occurs when $S = 1$ (platelets are perpendicular to the direction of permeation or planar arrangement of sheets).

Therefore, the Bharadwaj and MWS models produce functionally equivalent models of permeability for composite systems in which the dispersed phase is impermeable. The parameter n can be interpreted as the degree of "oblateness" for ellipsoidal particles or as a function of the aspect ratio and orientation for sheet-like particles. In this paper, the permeation experimental results were used to fit to the model in Eq. (1) to determine the shape factor (n) and the tortuosity factor (τ). The order parameter (S) was then determined based on the known aspect ratio L/W from TEM images.

Experimental

Materials

Neat PLLA from NatureWorks LLC with a molecular weight of about 100,000 g/mol was used as-received. Organically modified with a quaternary ammonium salt montmorillonite (MMT), Cloisite 30B, was provided by Southern Clay Product, Inc., Gonzales, TX, USA and used as-received. The extent of modification (ionic exchange) in Cloisite 30B is 90 meq/100 g clay. TGA technique showed that the percentages of inorganic and organic materials in MONT are 75 and 25 %, respectively.

Sample Preparation and Characterization

Neat PLLA pellets and MMT powder were dried in vacuum oven at 40 °C for 3 days prior to the melt-blending process. Melt mixing of neat PLLA and MMT was carried by a miniature batch mixer (MBM) adapted to a Haake Rheomix 600 and Rheocord 90 at the University of Calgary. The target was to produce composites at 2, 5, 7 and 10 wt% of MMT. For each concentration, melt-blending was performed at 185–190 °C for 4 min at a rotation speed of 30 rpm followed for another 4 min at 60 rpm. PLLA–MMT composite films of 500 microns in thickness were then prepared by compression-molding process, followed by rapid cooling in water while keeping the sample under the pressure. Neat PLLA without the presence of MMT was also processed by the MBM under the same conditions for the purpose of comparison. To prepare annealed (semicrystalline) samples, PLLA–MMT composite films were heat-treated in a conventional oven at different heat treatment conditions. TGA was used to measure the concentration of MMT in each PLLA–MMT composite films.

Wide-Angle X-ray Scattering (WAXD)

Wide–angle X-ray diffractograms (WAXD) of neat PLLA and PLLA–MMT composites were obtained by a Siemens D500 powder diffractometer using 1,500 W Cu anode with a Ni filter to produce a $Cu_{k\alpha}$ monochromatic wavelength of 1.54 Å (40 kV and 30 mA) in the 2θ range of 4–25° at a scanning speed of 0.3°/min. An X-ray diffractogram of as-received Cloisite 30B powder was also obtained.

Transmission Electron Microscopy (TEM)

One compression molded specimen of 5 wt% PLLA–MMT composite sample was ultra-cryomicrotomed to sections of ~70 nm at −40 °C using a Leica EM UC6 and EM FC6 cryochamber. TEM analysis of the nanocomposites was carried out from ultra-cryomicrotomed sample sections without staining on copper grids using a Tecnai F20 TEM at an accelerating voltage of 200 kV. TEM images were collected from different regions of three different sections.

Differential Scanning Calorimetry (DSC)

The glass transition, crystallization and melting temperatures of neat PLLA and PLLA–MMT composites with different concentrations of MMT were studied on a TA-Instruments (New Castle, DE, USA) differential scanning calorimeter (DSC)-model Q2000 series under constant nitrogen flow. All the DSC samples weighed about 4–5 mg. Tested samples were first heated from room temperature to 200 °C at 10 °C/min and held at 200 °C for 2 min before being cooled to 0 °C to remove any thermal history or crystallinity. After that, samples were heated again to 200 °C at a scanning rate of 10 °C/min in a second heating scan. The glass transition temperature of all samples was determined from the second heating scan while the crystallization and melting temperatures were determined from the first heating scan. Crystallinity of tested neat PLLA samples was determined by taking the ratio of the difference between the melting enthalpy and crystallizing enthalpy of the semicrystalline polymer to the theoretical melting enthalpy of 100 % crystalline PLA. 93 J/g was used for the melting enthalpy of 100 % crystalline PLA [5, 7]

$$\%crystallinity = \left(\frac{\Delta H_{melt} - \Delta H_{crys}}{93\text{J/g}}\right) \times 100\%. \qquad (6)$$

Crystallinity of tested PLLA–MMT composite samples was normalized by crystallinity of neat PLLA based on the concentration of MMT. For each concentration of MMT, at

least three samples were tested and the reported DSC results are the average of all trials.

Thermal Gravimetric Analysis (TGA)

TGA was done on neat PLLA and PLLA–MMT composite samples at different concentrations of MMT by using a TA-Instruments (New Castle, DE, USA) TGA-model Q50 series under constant nitrogen flow. For each tested sample, the temperature at which 95 wt% of the sample weight remains (5 wt% decomposition temperature) was determined to compare the thermal stability of PLLA–MMT composites at different concentrations of MMT.

Water Permeation Experiments

Permeation of water through neat PLLA and PLLA–MMT composite films was studied by an upright cup method in an environmental chamber with constant temperature and relative humidity [22]. Twenty mL vials with open-top caps and Teflon-lined septa with a 14-mm hole cut in the center of the septa were used. Membranes were cut into circles and placed inside the cap. Thickness was measured at 10–15 different points on the membrane by a digital micrometer. Vials were filled with 10 mL of water, covered by the cap with neat PLLA or PLLA–MMT composite membrane, and placed inside the environmental chamber. Vials were weighed every 24 h to determine the mass loss with time. When the vapor transfer rate per unit area (VTR) changed by <2 % within 24 h, the VTR was considered constant, and the permeability of water through the membrane was calculated by the following equation [22]:

$$P = \frac{L \times VTR}{S \times (P_1 - P_2)} \qquad (7)$$

where S is the saturation vapor pressure at the test temperature, P_1 is the relative humidity on the entrance side, P_2 is the relative humidity on the exit side and L is the sample thickness. VTR is defined as the ratio of the weight of the penetrant and the product of time and cross-sectional area. For all experiments reported in this study, the environmental chamber was kept under a temperature of 25 °C and a relative humidity of 30 % by using saturated salt solutions.

Results and Discussion

Morphological and Thermal Analysis

Figure 1 shows WAXS patterns of the MMT powder, the neat PLLA and the compression-molded PLLA–MMT composite films at 5 wt% of MMT. Both neat PLLA and
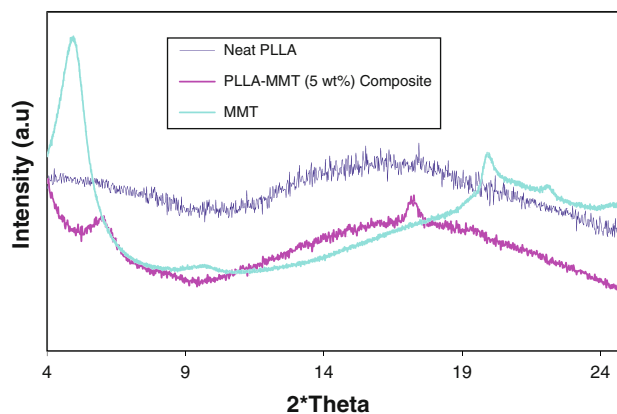

Fig. 1 WAXS pattern of MMT and PLLA–MMT composite at 5 wt% of MMT

PLLA–MMT composite samples were nearly amorphous. There was only one small crystalline PLLA peak at around 17.3° in the PLLA–MMT composite sample while an amorphous halo between 10 and 25° appeared in both neat PLLA and PLLA–MMT composite samples. MMT powder has two characteristic crystalline peaks: a high intensity primary peak at 4.8° corresponding to a d-spacing of 1.84 nm and a low intensity secondary peak at 9.6° corresponding to a d-spacing of 0.92 nm. In the WAXS pattern of the PLLA–MMT composite sample, there is only one peak at 6.1° corresponding to a d-spacing of 1.45 nm. The disappearance of the primary peak of MMT at 4.8° is presumably caused by the exfoliation of MMT platelets with good surface modification into the PLLA matrix. However, the secondary peak at 9.6° was shifted to 6.1°, which indicates that the polymer was also partially intercalated in between the layers of MMT platelets. The WAXS results therefore demonstrate that the structure of melt-blended PLLA–MMT composites was mostly exfoliation and partial intercalation. Similar results were found by Wong et al. [23]. The intercalation of MMT platelets might also have come from a small portion of MMT particles that remained unmodified during the surface modification process. Ray and Okamoto [24] also reported different structures of PLLA-organomodified clay nanocomposites, depending on the types of clays. It was shown that both intercalated and exfoliated structures exist in PLA-synthetic fluorine mica composites [24].

Figure 2 shows TEM images of PLLA–MMT composite film at 5 wt% of MMT. In these images, MMT platelets appear dark and are generally well-dispersed although there are some small aggregates of the MMT platelets. The TEM and WAXS results are consistent because both show exfoliation of modified MMT platelets and a small portion of aggregates which are presumably unmodified MMT platelets intercalated by the polymer. ImageJ software was used to estimate the dimensions of MMT platelets by
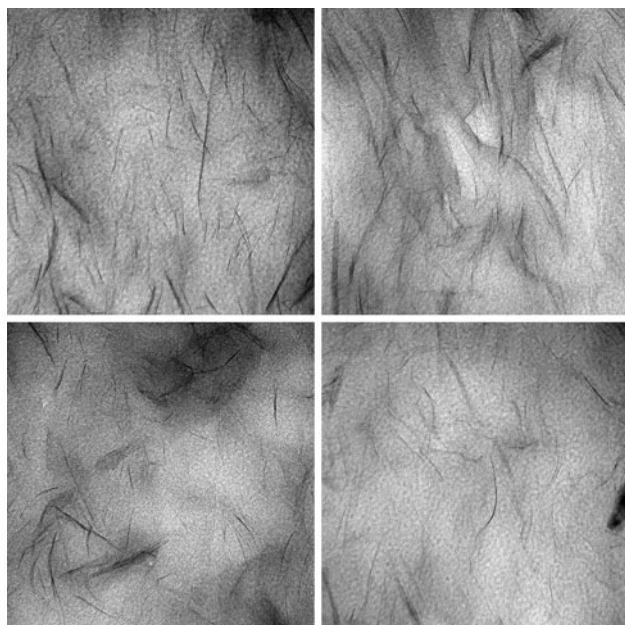
Fig. 2 TEM images of PLLA–MMT composite film with 5 wt% of MMT (dimensions of 586.8 × 586.8 nm)

analyzing the TEM images. The length (L) was found to be 92.3 ± 13.3 nm while the width (W) was found to be 1.77 ± 0.46 nm. The length (L) and width (W) values were averaged from at least 40 single platelets on each TEM image in Fig. 2.

The glass transition temperature, crystallization temperature, melting temperature, 5 wt% decomposition temperature, crystallization enthalpy, melting enthalpy and percentage of crystallinity of neat PLLA and PLLA–MMT composite samples are recorded in Table 1. Tested samples without heat treatment have a very low crystallinity (<7 %) or are nearly amorphous. This low crystallinity of tested samples was expected due to the fast water cooling process after the compression-molding process was performed. The glass transition temperatures of PLLA did not change significantly with the presence of MMT particles. The crystallization temperature decreased with the increase in MMT concentration until the concentration of MMT reached 5 wt% and remained stable at higher concentrations of

MMT. The melting temperature showed a slight trend of decreasing with increasing MMT concentration.

The 5 wt% decomposition temperature from TGA of composite samples increased with increasing the concentration of MMT below a concentration of 5 wt%, indicating that MMT particles were well dispersed in the PLLA matrix. However, as the concentration of MMT went beyond 5 wt%, the temperature of 5 wt% decomposition started to decrease. Specifically, the temperature of 5 wt% decomposition of composites at 7 and 10 wt% of MMT were found to be 330.7 and 323.0 °C, respectively. This result indicates that dispersion of MMT particles in the polymer matrix became difficult at higher concentrations of MMT. Therefore, fabrication of composites at higher concentrations of MMT than 10 wt% was not carried out in this research.

Permeation Results

Permeation experiments were carried out on neat PLLA and PLLA–MMT composite samples by the procedure described in the experimental section. In this section, all samples are nearly amorphous because they were quickly quenched after melt pressing without further heat treatment. Table 2 shows the permeability of neat PLLA and PLLA–MMT composites at various MMT concentrations. MMT concentration was converted from wt% to volume fraction by using the density of PLLA and MMT provided

Table 2 Water permeation in neat PLLA and PLLA–MMT composite samples without heat treatment at different concentrations of MMT

MMT wt%	MMT volume fraction	Permeability [10^{-10} cm^3 (STP) cm/cm^2 s Pa]
0	0.0000	6.34 ± 0.60
2	0.0126	5.70 ± 0.52
5	0.0319	5.17 ± 0.45
7	0.0500	4.56 ± 0.43
10	0.0651	4.21 ± 0.41

Table 1 Thermal properties and crystallinity of neat PLLA and PLLA–MMT composite samples without heat treatment

MMT wt%	T_g (°C)	T_c (°C)	T_m (°C)	ΔH_{crys} (J/g)	ΔH_{melt} (J/g)	Crystallinity (%)	5 wt% decomposition temperature (°C)
0	60.8	105.5	169.2	1.43	7.19	6.2	320.2
2	60.3	101.3	169.0	31.1	37.1	6.6	329.5
5	60.1	98.2	167.4	29.9	30.5	0.6	332.8
7	60.4	97.1	168.2	31.4	34.1	3.1	330.7
10	59.0	98.4	166.7	31.0	36.1	6.1	323.0

T_c, T_m, ΔH_{crys}, ΔH_{melt} and crystallinity were calculated from the first heating cycles while T_g was calculated from the second heating cycle

by NatureWorks LLC and Southern Clay Products, Inc. According to these results, the water permeability in PLLA–MMT composites reduced with increasing MMT concentration. At 5 wt% (0.032 volume fraction) and 10 wt% (0.065 volume fraction) of MMT, water permeation in PLLA–MMT composite decreased by about 19 and 34 % compared with neat PLLA, respectively. The addition of MMT particles increases the tortuosity of the pathway for water molecules to pass through the polymer membrane. This result showed that the presence of MMT particles significantly improves the moisture barrier properties in PLA. At high concentrations (10 wt%) of MMT, the dispersion of clay particles into the PLLA matrix is more difficult and some aggregation of MMT particles was observed on the surface of the composite film. Therefore, to maintain good clay dispersion, melt-blending experiments were not carried out with concentrations higher than 10 wt% of MMT. The relationship between MMT concentration and water permeability in the composite membrane is not linear (see Fig. 3). A combination of factors, such as the platelet orientation, aspect ratio and concentration of MMT particles in the polymer matrix affect the water permeation of the composite membrane as discussed in the next section.

Application of the Maxwell–Wagner–Sillars (MWS) and Bharawaj's Models

Nonlinear regression of Eq. (1) to fit the data in Table 2 and Fig. 3 predicts a shape factor (n) of 0.87. By the MWS model, $n = 0.87$ indicates that MMT particles are of oblate ellipsoidal shape with high aspect ratio which is consistent with fully exfoliated MMT platelets in the PLLA matrix.
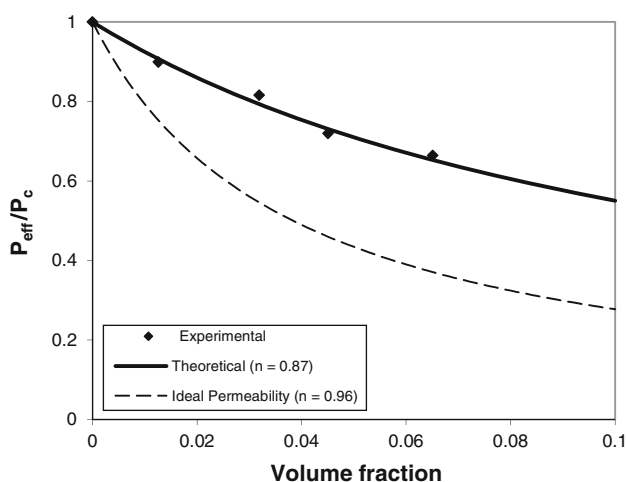

Fig. 3 A comparison between water permeation experimental results and model in PLLA–MMT composite samples (all data were taken at 25 °C and 30 % relative humidity)

By Bharadwaj's model, $n = 0.87$ combined with the aspect ratio of $L/W = 52.1$ from TEM images produces an order parameter S of approximately -0.03, which corresponds to randomly-oriented platelets. By taking into account the uncertainties of L and W measurements from TEM images, the order parameter S ranges between -0.15 and 0.2. The interpretation of the parameters from both models is consistent. The MWS provides information regarding the shape of the platelets while the Bharawaj's model provides the information regarding the orientation of the platelets in the polymer matrix. The best moisture barrier properties are expected from an exfoliated dispersion of MMT in PLLA. From the TEM images in Fig. 2, at a concentration of 5 wt% of MMT, an exfoliated structure was observed. The "flat-sheet-like" structure of MMT as a result of exfoliation also matched with a shape factor of 0.87 which indicates oblate ellipsoidal shape in the MWS model.

Both the MWS and Bharawaj's models are consistent in estimating the shape and orientation of the MMT platelets in the PLLA matrix which matches with the results from TEM images. The water permeability in a composite membrane depends on the platelet aspect ratio and orientation. High aspect ratio and random exfoliation are desired factors to improve the water barrier properties in PLLA–MMT composites. The ideal case for the best moisture barrier properties of the composites occurs when $S = 1$ ($\theta = 90$ °C or planar arrangement of sheets). Assuming that the aspect ratio L/W is fixed at 52.1, by orienting the platelets, it could be possible to increase the order parameter S to approximately one and achieve the best barrier properties. Comparisons between theoretical prediction and permeation experimental results corresponding to $n = 0.87$, $L = 92.3$ nm, $W = 1.77$ nm and $S = 0$ is shown in Fig. 3. A curve corresponding to ideal permeation that is achieved with planar arrangement of sheets ($S = 1$ and $n = 0.96$) is also shown in Fig. 3. When the platelets are aligned perpendicular to the direction of permeation, it could lead to significant further reductions in permeability.

The Effect of Heat Treatment on Water Permeation of PLLA–MMT Composites

The previous section pertained only to water permeation in nearly amorphous composite samples. However, prior research showed that crystallinity affects water permeability in polymers [3, 11, 25–29]. Table 3 shows the change of water permeation and crystallinity of composites with 5 wt% MMT as a function of different heat treatment conditions. Water permeation values shown in Table 3 are averages of 4–5 different experiments. After compression-molding, these PLLA–MMT composite films were treated at different temperatures to create semi-crystalline films. The water permeability of neat PLLA has been measured

Table 3 Water permeation in PLLA–MMT composite sample with 5 wt% of MMT at different heat treatment conditions

C30B wt%	Heat treatment	Crystallinity (%) [from DSC]	Permeability [10^{-10} cm^3 (STP) cm/cm^2 s Pa]
5	No heat treatment	0.63	5.17 ± 0.52
5	70 °C–12 h	42.2	4.95 ± 0.50
5	90 °C–1 h	39.1	4.65 ± 0.47
5	120 °C–1 h	41.7	5.02 ± 0.50

by other researchers [30] and the results in this study showed a good agreement with literature.

For the three heat treatment regimes in Table 3, the samples exhibited similar crystallinity (between 39 and 42 %). Similar results of crystallinity in composite samples prepared by the solvent-casting method were also shown in our previous publication [25]. Within the error range of the experiments, the difference between water permeability in heat-treated PLLA–MMT composite samples is insignificant. This result contradicts the common trend that gas permeability in semi-crystalline polymers is lower than in amorphous polymers, a trend that is due to the impermeable crystallites increasing the tortuosity of the transport pathway for the gas molecules [29, 31]. In the PLLA–MMT composite samples shown here, permeability is independent of the total percentage of crystallinity.

Discussion of Water Permeability, Solubility and Diffusivity in Neat PLLA and PLLA–MMT Composites

In one of our publications, the water sorption in neat PLLA and PLLA–MMT composites fabricated by the solution–casting method was explored [25]. The results showed that at the same heat treatment condition, the amount of water sorption in PLLA–MMT composite was about 20 % higher than that in neat PLLA partially due to the presence of the hydrophilic hydroxyl (OH) group in the organic modifier of MMT [25]. However, although the solubility of water increased, the data in Table 2 shows that the permeability of water in PLLA–MMT composite with 5 wt% of MMT is lower than that in neat PLLA. By assuming that the "solution–diffusion" model applies [26, 28], permeability is a product of solubility and diffusivity ($P = S \times D$ where P, S and D stand for permeability, solubility and diffusivity, respectively). Because the addition of 5 wt% of MMT particles in the PLLA matrix led to an increase of 20 % in the water sorption (solubility) while the water permeability decreased 20 %, it can be inferred that the diffusivity decreased by about 33 %. This result is consistent with the presence of MMT platelets that

can increase the tortuosity of the pathway for water molecules travelling through the membrane.

The change in water permeability by varying heat treatment conditions observed for composite PLA in this paper is small compared with the change in water sorption for composite PLA fabricated by the solution–casting method. Specifically, as reported in our previous publication, water sorption in PLLA–MMT composites with 5 wt% of MMT increased with heat treatment temperature until 120 °C. Above 120 °C, the change in water sorption became negligible. At an optimized heat treatment temperature of 90 °C, the water sorption reduced 25 % compared with other heat treatment conditions [25]. By the assumption of the solution–diffusion model [26, 28], these results indicate that the diffusivity in PLLA–MMT composites increases with heat treatment temperature until reaching a saturated level.

Conclusions

PLLA–MMT composite films at different concentrations of MMT were fabricated by melt-blending and compression molding. Permeability measurements show that the water permeation in PLLA–MMT composites decreases with increasing concentration of MMT. At a concentration of 10 wt% of MMT, the water permeation in composites is about 34 % less than in neat polymer. WAXS and TEM results indicate that most of the MMT particles are generally well-dispersed and randomly exfoliated. TEM images also show that MMT platelets have high aspect ratios and random orientation. DSC results show that the T_g and T_m are somewhat insensitive to the concentration of MMT while T_c has a decreasing trend at higher concentrations of MMT.

The permeation results were regressed to a model for permeability of composites that produced a shape factor of $n = 0.87$. This shape factor corresponds to high aspect ratio particles with random orientation. The permeation results are consistent with highly-exfoliated clay particles as observed in TEM and WAXS. In conclusion, fabricating PLLA nanocomposites with montmorillonite increases the amount of water sorption but decreases the rate of water permeation in PLLA. By the solution–diffusion model, the effective diffusion coefficient of water in composites is much lower than that in neat PLLA due to the increased tortuosity caused by the presence of clay platelets.

References

1. Garlotta D (2001) J Polym Environ 9:63–84
2. Oliveira NS, Dorgan J, Coutinho JAP, Ferreira A, Daridon JL, Marrucho IM (2007) J Polym Sci Pol Phys 45:616–625
3. Oliveira NS, Goncalves CM, Coutinho JAP, Ferreira A, Dorgan J, Marrucho IM (2006) Fluid Phase Equilib 250:116–124
4. Oliveira NS, Oliveira J, Gomes T, Ferreira A, Dorgan J, Marrucho IM (2004) Fluid Phase Equilib 222:317–324
5. Cairncross RA, Ramaswamy S, O'Connor R (2007) Int Polym Process 22:33–37
6. Harada M, Iida K, Okamoto K, Hayashi H, Hirano K (2008) Polym Eng Sci 48:1359–1368
7. Otsuka H, Nagasaki Y, Kataoka K (2000) Biomacromolecules 1:39–48
8. Tsuji H, Muramatsu H (2001) J Appl Polym Sci 81:2151–2160
9. Gorrasi G, Tammaro L, Vittoria V, Paul MA, Alexandre M, Dubois P (2004) J Macromol Sci Phys B43:565–575
10. Krikorian V, Pochan DJ (2003) Chem Mater 15:4317–4324
11. Koo D, Du A, Palmese GR, Cairncross RA (2012) Polym Chem UK 3:9
12. Pluta M, Galeski A, Alexandre M, Paul MA, Dubois P (2002) J Appl Polym Sci 86:1497–1506
13. Zenkiewicz M, Richert J (2008) Polym Test 27:835–840
14. Bharadwaj RK (2001) Macromolecules 34:9189–9192
15. Bouma RHB, Checchetti A, Chidichimo G, Drioli E (1997) J Membr Sci 128:141–149
16. Chung TS, Jiang LY, Li Y, Kulprathipanja S (2007) Prog Polym Sci 32:483–507
17. Gonzo EE, Parentis ML, Gottifredi JC (2006) J Membr Sci 277:46–54
18. Mahajan R, Koros WJ (2002) Polym Eng Sci 42:1420–1431
19. Moore TT, Koros WJ (2005) J Mol Struct 739:87–98
20. Moore TT, Mahajan R, Vu DQ, Koros WJ (2004) AIChE J 50:311–321
21. Pal R (2008) J Colloid Interf Sci 317:191–198
22. Napadensky E, Elabd YA (2004) Breathability and Selectivity of Selected Materials for Protective Clothing, ARL-TR-3235, July 2004
23. Wong W-K, Cheng S, Li CY, Ahmad I, Cairncross R, Hsuan YG (2012) Polym Degrad Stab 97:192–199
24. Ray SS, Okamoto M (2003) Macromol Rapid Commun 24:815–840
25. Du A, Koo D, Ziegler M, Cairncross RA (2011) J Polym Sci Part B Polym Phys 49:873–881
26. Komatsuka T, Kusakabe A, Nagai K (2008) Desalination 234:212–220
27. Koo D, Du A, Palmese GR, Cairncross RA (2012) Polymer 53:1115–1123
28. Siparsky G, Voorhees K, Dorgan J, Schilling K (1997) J Polym Environ 5:125–136
29. Vittoria V (1995) J Mater Sci 30:3954–3958
30. Auras RA, Harte B, Selke S, Hernandez R (2003) J Plast Film Sheet 19:123–135
31. Drieskens M, Peeters R, Mullens J, Franco D, Lemstra PJ, Hristova-Bogaerds DG (2009) J Polym Sci Pol Phys 47:2247–2258